Presented at the Conference in Honor of Bob Taylor, Palo Alto, CA.

RECENT RESULTS ON THE NUMERICAL INTEGRATION OF INFINITE-DIMENSIONAL HAMILTONIAN SYSTEMS

J.C. Simo and O. Gonzalez

Division of Applied Mechanics, Department of Mechanical Engineering, Stanford University, Stanford, CA 94305, USA

Dedicated to Bob Taylor on the occasion of his 60^{th} birthday.

ABSTRACT

This paper summarizes some recent results on symplectic and energy-momentum conserving time-stepping algorithms for Hamiltonian systems in nonlinear solid mechanics. To motivate conserving schemes a numerical example is provided in which a typical symplectic method is shown to exhibit blow-up, i.e., instability. Some new analytical results on the observed instability are then briefly presented. In particular, results are presented which show that within the context of a simple model problem the implicit mid-point rule (the prototypical symplectic implicit Runge-Kutta method) is only conditionally stable while a conserving scheme is unconditionally (spectrally) stable. An example is then given which shows that the approach used to construct the conserving algorithm for the model problem generalizes to more complex systems such as nonlinear elastodynamics. With regard to higher-order conserving schemes, a method by which fourth-order accuracy may be obtained from a large class of second-order schemes is summarized.

1. INTRODUCTION.

In recent years there has been much interest in the long-term simulation of nonlinear Hamiltonian systems. In particular, infinite-dimensional systems arising in solid mechanics such as nonlinear elastodynamics, rods, and shells. From a numerical analysis standpoint the design of time-stepping algorithms for these systems is difficult since the issue of stiffness has to be addressed in the absence of numerical dissipation (i.e., if a scheme is to inherit any of the key properties of a Hamiltonian system it must be dissipationless). Given that stiffness is an issue and that one is interested in long-term simulations it is then natural to search for implicit schemes which are unconditionally stable and which preserve as much as possible the intrinsic properties of the underlying system. Namely, conservation laws such as that of

energy and angular momentum (arising from symmetries in the Hamiltonian relative to a group of transformations on the phase space) and the symplectic character of the exact flow, both of which play a central role in the qualitative behavior of the long-term dynamics. This leads one to consider two basic classes of implicit integration schemes for Hamiltonian systems: the so-called symplectic integrators which preserve exactly the symplectic character of a Hamiltonian flow† (for examples see [1]-[5]) and the energy-momentum (or conserving) algorithms which by design preserve the constants of motion; see [6]-[11].

In this paper we review some recent results on symplectic and conserving algorithms. We first motivate the need for conserving schemes via a numerical example from nonlinear elastodynamics. This example illustrates the disappointing results produced by symplectic schemes, the implicit mid-point rule in particular. We then briefly review some analytical results showing that the observed behavior is typical, i.e., that the implicit mid-point rule exhibits spurious solutions and is unstable even for the simplest nonlinear system: Kepler's problem. Within the context of this model problem the cause of the instability is identified and it is shown that one way to preclude instability is to use an alternative conserving algorithm. We then show how the idea of a conserving algorithm may be generalized from the simple model problem to a more complex system such as elastodynamics. In particular, we show how to construct a conserving algorithm for general frame-invariant hyperelastic models in nonlinear elasticity. Finally we discuss results on a general technique by which fourth-order accuracy may be obtained from a large class of second-order schemes.

2. MOTIVATION: A NUMERICAL EXAMPLE.

In this section we present a numerical example in which a symplectic method, the implicit mid-point rule, is used to numerically integrate the equations of motion for nonlinear elastodynamics, a typical infinite-dimensional Hamiltonian system. The goal here is to motivate the need for alternative schemes.

2.1. Weak Formulation.

Let $\mathcal{B} \subset \mathbb{R}^{n_{\rm dim}}$ denote the reference placement of a continuum body, where $1 \leq n_{\rm dim} \leq 3$ is the spatial dimension, with smooth boundary $\partial\mathcal{B}$. In accordance with a Lagrangian description of the motion material points are labeled throughout by their position $\boldsymbol{X} \in \mathcal{B}$ in the reference placement and we consider the reference boundary $\partial\mathcal{B}$ to be partioned into disjoint subsets such that $\partial\mathcal{B} = \overline{\Gamma_\varphi \cup \Gamma_\sigma}$ with $\Gamma_\varphi \cap \Gamma_\sigma = \emptyset$. We denote by $\boldsymbol{\varphi}_t : \mathcal{B} \to \mathbb{R}^{n_{\rm dim}}$ an element of a t-parameter family of deformations from the reference placement onto the current placement which for

† It can be shown that this is true only in the canonical case when the symplectic two-form is constant; see [12].

each $t \in \mathbb{R}_+$ is an element of the configuration space

$$Q = \{\boldsymbol{\varphi}_t : \mathcal{B} \to \boldsymbol{R}^{n_{\rm dim}} \mid J(\boldsymbol{\varphi}_t) = \det[D\boldsymbol{\varphi}_t] > 0 \text{ and } \boldsymbol{\varphi}_t|_{\Gamma_\varphi} = \bar{\boldsymbol{\varphi}}_t\}, \tag{2.1}$$

where $D(\cdot) = \partial(\cdot)/\partial \boldsymbol{X}$ and $\bar{\boldsymbol{\varphi}}_t$ is specified data on Γ_φ. Let $\mathcal{V} = TQ$ be the space of admissible variations associated with the configuration space Q, i.e.

$$\mathcal{V} = \{\boldsymbol{\eta} : \mathcal{B} \to \boldsymbol{R}^{n_{\rm dim}} \mid \boldsymbol{\eta}|_{\Gamma_\varphi} = \boldsymbol{0}\}, \tag{2.2}$$

then the weak form of balance of momentum at time $t \in \mathsf{I}$ takes the form

$$\langle \dot{\boldsymbol{\pi}}_t, \boldsymbol{\eta} \rangle + \langle D\boldsymbol{\varphi}_t \boldsymbol{S}_t, \textsc{Grad}[\boldsymbol{\eta}] \rangle = \langle \boldsymbol{f}_t, \boldsymbol{\eta} \rangle + \langle \bar{\boldsymbol{t}}_t, \boldsymbol{\eta} \rangle_\Gamma \qquad \forall \boldsymbol{\eta} \in \mathcal{V}, \tag{2.3}$$

where $\bar{\boldsymbol{t}}_t$ is the prescribed nominal traction vector, $\boldsymbol{f}_t$ is a prescribed body force per unit reference volume, $\boldsymbol{V}_t = \dot{\boldsymbol{\varphi}}_t$ is the material velocity field, $\boldsymbol{\pi}_t = \rho_0 \boldsymbol{V}_t$ is the canonical momenta, $\rho_0 : \mathcal{B} \to \mathbb{R}_+$ is the reference density of the continuum body, and $\boldsymbol{S}_t$ is the *symmetric Piola-Kirchhoff* or *convected* stress tensor defined in terms of a stored energy function $W(\boldsymbol{C}(\boldsymbol{\varphi}_t))$ by

$$\boldsymbol{S}_t = 2\nabla W(\boldsymbol{C}(\boldsymbol{\varphi}_t)) \quad \text{where} \quad \boldsymbol{C}(\boldsymbol{\varphi}_t) = D\boldsymbol{\varphi}_t^{\rm T} D\boldsymbol{\varphi}_t \tag{2.4}$$

is the right Cauchy-Green deformation tensor. Here $\langle \cdot\ , \cdot \rangle$ and $\langle \cdot\ , \cdot \rangle_\Gamma$ denote the L_2–inner product on $\mathcal{B}$ and Γ_σ, respectively, of scalars, vectors, or tensors depending on the context and $\textsc{Grad}[\cdot]$ denotes the gradient operator relative to a coordinate system on the reference placement $\mathcal{B} \subset \mathbb{R}^{n_{\rm dim}}$.

Here we note that for the pure Neumann problem ($\Gamma_\varphi = \emptyset$) under equilibrated loading the dynamics described by (2.3) possess the conservation laws of total linear and angular momentum and total energy.

2.2. Mid-Point Approximation.

Consider a partition $\{t_n\}_{n=0,1,\ldots,N}$ of the time interval I of interest into non-overlapping subintervals $[t_n, t_{n+1}]$ with $\Delta t = t_{n+1} - t_n > 0$ $(n = 0, 1, \ldots, N)$. Given $\boldsymbol{\varphi}_n : \mathcal{B} \to \mathbb{R}^{n_{\rm dim}}$ and $\boldsymbol{\pi}_n : \mathcal{B} \to \mathbb{R}^{n_{\rm dim}}$ the algorithmic problem is to compute $\boldsymbol{\varphi}_{n+1}$ and $\boldsymbol{\pi}_{n+1}$ and generate a solution sequence $\{\boldsymbol{\varphi}_n, \boldsymbol{\pi}_n\}_{n=0,1,\ldots,N}$. To this end we consider the following mid-point approximation to the weak form of the momentum balance (2.3):

$$\begin{aligned} \frac{1}{\Delta t}\langle \boldsymbol{\pi}_{n+1} - \boldsymbol{\pi}_n, \boldsymbol{\eta} \rangle + \langle D\boldsymbol{\varphi}_{n+\frac{1}{2}} \boldsymbol{S}, \textsc{Grad}[\boldsymbol{\eta}] \rangle \\ = \langle \boldsymbol{f}_{n+\frac{1}{2}}, \boldsymbol{\eta} \rangle + \langle \bar{\boldsymbol{t}}_{n+\frac{1}{2}}, \boldsymbol{\eta} \rangle_\Gamma \quad \forall \boldsymbol{\eta} \in \mathcal{V}, \end{aligned} \tag{2.5a}$$

along with the local relations

$$\frac{1}{\Delta t}[\boldsymbol{\varphi}_{n+1} - \boldsymbol{\varphi}_n] = \boldsymbol{V}_{n+\frac{1}{2}} \qquad \text{and} \qquad \boldsymbol{\pi}_{n+\frac{1}{2}} = \rho_0 \boldsymbol{V}_{n+\frac{1}{2}}, \tag{2.5b}$$

where $(\cdot)_{n+\frac{1}{2}} = \frac{1}{2}[(\cdot)_n + (\cdot)_{n+1}]$ and the stress field is evaluated at the mid-point configuration as

$$\boldsymbol{S} = 2\nabla W(\boldsymbol{C}(\boldsymbol{\varphi}_{n+\frac{1}{2}})). \tag{2.6}$$

Under the same conditions as in the exact case, the time-discrete dynamics described by (2.5a,b) together with (2.6) possess the conservation laws of total linear and angular momentum. Note that while the symplectic mid-point approximation inherits the conservation laws of momentum from the underlying system it cannot in general conserve energy since it is symplectic [13].

To complete the discretization we perform a standard spatial Galerkin projection of the time-discrete weak form into a finite-dimensional phase space $P^h \subset P$. It can be verified that for elastodynamics the Galerkin finite element projection preserves the conservation properties of the time-discrete dynamics.

2.3. A Numerical Simulation.

For our example we consider the dynamics of an elastic L-shaped block subject to no boundary restrictions with material response governed by a Saint Venant-Kirchhoff elastic model. After an initial loading phase the body tumbles free of external forces in the ambient space undergoing finite deformation accompanied by large overall rotations and translations. The sequence of deformed shapes obtained in the course of the simulation is shown in Figure 2.1 without any magnification of the actual deformations.

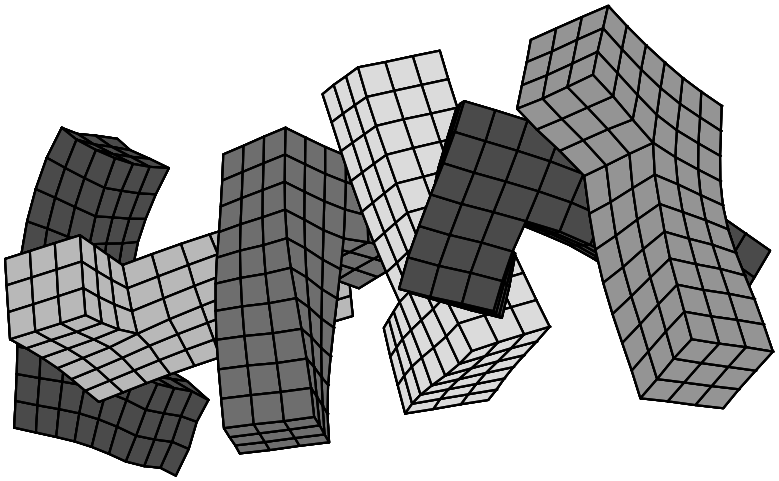

FIGURE 2.1 Sequence of deformed shapes for the tumbling L-shaped block.

The plots shown in Figure 2.2 contain the time histories of the total energy and the three components of the total angular momentum computed with the symplectic midpoint-rule. The time history of the total linear momentum is not reported since

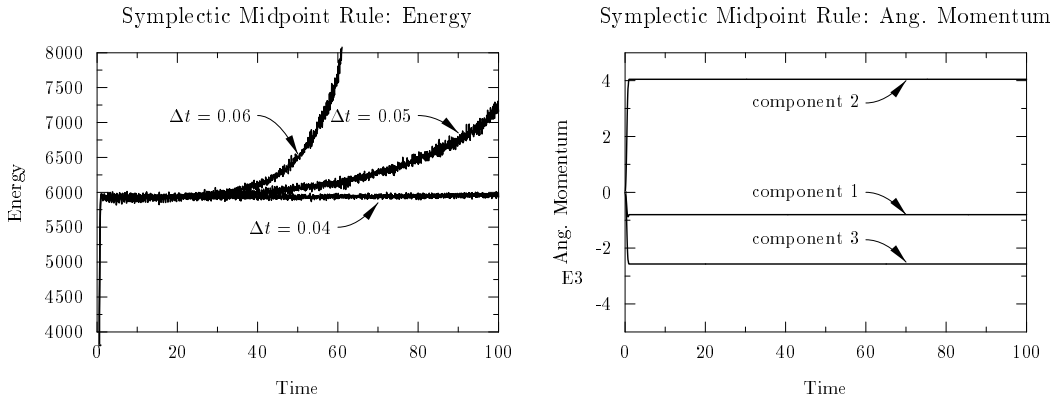

FIGURE 2.2 Time histories of the total angular momentum and the total energy computed with the symplectic mid-point rule.

this is trivially preserved by any consistent algorithm. The results shown in Figure 2.2 include computations with several step-sizes and demonstrates that solutions computed with the symplectic mid-point rule may exhibit significant energy growth for the larger time-step sizes which in long-term calculations leads to an eventual blow-up of the algorithmic solution. This strongly suggests a loss of the unconditional stability property of this method in the nonlinear regime.

3. ANALYSIS OF THE INSTABILITY PROBLEM.

In this section we review some analytical results pertaining to the observed instability of the symplectic mid-point rule, the prototypical symplectic implicit Runge-Kutta method. Within the context of a simple model problem we identify the cause of the observed instability as spurious coupling between group and internal motions and present two ways to avoid this phenomena. Our basic strategy here is to analyze a system for which we can obtain exact algorithmic solutions (in particular, fixed points) and then analyze the stability of these solutions. To this end, we consider the simplest possible nonlinear system possessing the conservation laws of energy and angular momentum: the classical problem of a particle moving in $\mathbb{R}^3$ under the influence of a central force field. The potential function is ultimately chosen to describe the situation typically found in spatial discretizations of infinite-dimensional Hamiltonian systems. Namely, a wide frequency content with response dominated by the lower spectrum. For details and proofs we refer the reader to [14].

3.1. Problem Formulation and Conservation Laws.

Consider a single particle of mass $m > 0$ in $\mathbb{R}^3$ moving about a fixed center of

force which will be taken as the origin of an inertial coordinate system and denote the position of the particle by $\boldsymbol{q} \in \mathbb{R}^3$. We restrict ourselves to conservative central forces with potential $V : \mathbb{R}^3 \to \mathbb{R}$ where the potential is by necessity a function of the radial distance $|\boldsymbol{q}|$ only. This problem has a well-known Hamiltonian structure which we summarize below.

Let $\boldsymbol{z} = (\boldsymbol{q}^{\mathrm{T}}, \boldsymbol{p}^{\mathrm{T}})^{\mathrm{T}} \in P = \mathbb{R}^6$ where $\boldsymbol{p} = m\dot{\boldsymbol{q}}$ is the momenta conjugate to $\boldsymbol{q}$ and define the Hamiltonian function $H : P \to \mathbb{R}$ by

$$H(\boldsymbol{z}) = \frac{1}{2m}|\boldsymbol{p}|^2 + V(|\boldsymbol{q}|). \tag{3.1}$$

Hamilton's equations for a motion $t \mapsto \boldsymbol{z}(t) \in P$ then take the form

$$\left.\begin{aligned} \dot{\boldsymbol{q}} &= \quad m^{-1}\boldsymbol{p}, \\ \dot{\boldsymbol{p}} &= -\frac{V'(|\boldsymbol{q}|)}{|\boldsymbol{q}|}\boldsymbol{q}. \end{aligned}\right\} \tag{3.2}$$

The dynamics described by equations (3.2) give rise to a flow on the phase space P with the following conservation laws. Define the angular momentum map $\boldsymbol{J} : P \to \mathbb{R}^3$ by $\boldsymbol{J}(\boldsymbol{z}) = \boldsymbol{q} \times \boldsymbol{p}$. Then the Hamiltonian H and momentum map $\boldsymbol{J}$ are conserved along solutions $t \mapsto \boldsymbol{z}(t) \in P$ of Hamilton's equations in the sense that

$$\frac{d}{dt}H(\boldsymbol{z}(t)) = 0 \quad \text{and} \quad \frac{d}{dt}\boldsymbol{J}(\boldsymbol{z}(t)) = \boldsymbol{0}. \tag{3.3}$$

3.2. Reduction and Stability.

Due to the presence of the conserved quantity $\boldsymbol{J}$ the dynamics may be formulated on a reduced phase space $\tilde{P} \subset \mathbb{R}^2$. In particular, the dynamics of the system on P can be shown to be completely characterized by the evolution of a set of reduced variables $(\lambda, \pi)^{\mathrm{T}} \in \tilde{P} \subset \mathbb{R}^2$ and a moving frame. (In this case the dynamics of the reduced variables is uncoupled from that of the moving frame.) The evolution equations for the reduced variables are

$$\left.\begin{aligned} \dot{\lambda} &= \quad \pi/m, \\ \dot{\pi} &= -V'(\lambda) + |\boldsymbol{\mu}|^2/m\lambda^3, \end{aligned}\right\} \tag{3.4}$$

where $\boldsymbol{\mu}$ is the angular momentum of the system (constant). Note that since the evolution of λ and π completely determine the motion of the system stability can be inferred from the reduced equations.

Let $\tilde{\boldsymbol{z}} = (\lambda, \pi)^{\mathrm{T}} \in \tilde{P} \subset \mathbb{R}^2$ and consider a fixed point $\tilde{\boldsymbol{z}}^* \in \tilde{P}$ of the reduced equations (3.4) given above. Clearly, the fixed point must be of the form $\tilde{\boldsymbol{z}}^* = (\lambda^*, 0)^{\mathrm{T}}$ where λ^* is a stationary point of the *amended potential* $V_\mu(\lambda) = V(\lambda) + |\boldsymbol{\mu}|^2/2m\lambda^2$.

Note that a fixed point of the reduced Hamiltonian flow on $\tilde{P}$ corresponds to a steady motion on the canonical phase space P and hence is called a *relative equilibria*. In terms of the motion of the particle, the relative equilibria corresponds to a steady circular orbit of the particle about the origin with radius $|\boldsymbol{q}| = \lambda^*$.

To examine the stability of the relative equilibria we linearize the reduced equations about the fixed point and examine the spectrum of the linearized t-advance mapping $\boldsymbol{A}_t = D\boldsymbol{F}_t(\tilde{\boldsymbol{z}}^*)$ where $\boldsymbol{F}_t : \tilde{P} \to \tilde{P}$ is the t-advance mapping for the reduced dynamics. Spectral stability of the fixed point $\tilde{\boldsymbol{z}}^* = (\lambda^*, 0)^{\mathrm{T}} \in \tilde{P}$ requires that the eigenvalues of $\boldsymbol{A}_t$ be on the unit circle in the complex plane. Since $\boldsymbol{F}_t$ is a symplectic map on $\tilde{P}$ for each $t \in \mathbb{R}$ and the reduced space is two-dimensional we have that stability may be inferred from the trace of $\boldsymbol{A}_t$.

3.3. Mid-Point Approximation.

Approximation in the Canonical Space. Let I be the time interval of interest and consider the equations of motion on P given in (3.2) with initial data $\boldsymbol{z}(0) = \boldsymbol{z}_0$. Given a partition $\{t_n\}_{n=0}^N$ of I such that $t_{n+1} - t_n = \Delta t > 0$, the algorithmic problem is to compute $\boldsymbol{z}_{n+1}$ from given data $\boldsymbol{z}_n \in P$ and generate a solution sequence $\{\boldsymbol{z}_n\}_{n=0,1,\ldots,N}$ where $\boldsymbol{z}_n$ stands for an algorithmic approximation to $\boldsymbol{z}(t_n)$. The mid-point approximation to (3.2) is

$$\left.\begin{aligned} \boldsymbol{q}_{n+1} - \boldsymbol{q}_n &= \Delta t m^{-1} \boldsymbol{p}_{n+\frac{1}{2}}, \\ \boldsymbol{p}_{n+1} - \boldsymbol{p}_n &= -\Delta t \frac{V'(|\boldsymbol{q}_{n+\frac{1}{2}}|)}{|\boldsymbol{q}_{n+\frac{1}{2}}|} \boldsymbol{q}_{n+\frac{1}{2}}. \end{aligned}\right\} \tag{3.5}$$

where $(\cdot)_{n+\frac{1}{2}} = \frac{1}{2}[(\cdot)_n + (\cdot)_{n+1}]$.

Reduction and Stability. As in the exact case the momentum map $\boldsymbol{J}$ is preserved along any motion $\{\boldsymbol{z}_n\}_{n=0,1,\ldots,N}$ defined by the mid-point algorithm (3.5). Hence the discrete dynamics may be reduced to the phase space $\tilde{P} \subset \mathbb{R}^2$. Performing the reduction we then seek, as in the exact case, a fixed point $\tilde{\boldsymbol{z}}^\star \in \tilde{P}$ of the reduced algorithmic equations. Stability is then determined by linearizing about the fixed point and examining the eigenvalues of the amplification matrix. This leads to the following results:

1) The mid-point scheme formulated on the canonical phase space P possesses an algorithmic relative equilibria which depends on the time step.

2) The equilibria is only conditionally stable.

Approximation in the Reduced Space. To contrast the above results obtained by reducing the mid-point approximation on P, we formulate the mid-point algorithm directly on the reduced space $\tilde{P}$ and address the question of stability for this

formulation. The mid-point approximation to the reduced equations (3.4) is

$$\left.\begin{aligned} \lambda_{n+1} - \lambda_n &= \Delta t m^{-1} \pi_{n+\frac{1}{2}}, \\ \pi_{n+1} - \pi_n &= -\Delta t V'_\mu(\lambda_{n+\frac{1}{2}}). \end{aligned}\right\} \tag{3.6}$$

For this approximation we have the following results:

1) The scheme exactly preserves the fixed point in $\tilde{P}$.

2) The equilibria is unconditionally (spectrally) stable.

3.4. Energy-Momentum Approximation.

Approximation in the Canonical Space. As before, let $\boldsymbol{z}_n \in P$ denote an algorithmic approximation to $\boldsymbol{z}(t_n)$ and as a point of departure consider the following mid-point approximation to the equations of motion on P:

$$\left.\begin{aligned} \boldsymbol{q}_{n+1} - \boldsymbol{q}_n &= \Delta t m^{-1} \boldsymbol{p}_{n+\frac{1}{2}}, \\ \boldsymbol{p}_{n+1} - \boldsymbol{p}_n &= -\Delta t \sigma \boldsymbol{q}_{n+\frac{1}{2}}, \end{aligned}\right\} \tag{3.7}$$

where $\sigma \in \mathbb{R}$ is an algorithmic parameter and as usual $(\cdot)_{n+\frac{1}{2}} = \frac{1}{2}[(\cdot)_n + (\cdot)_{n+1}]$. Here we note that the above algorithm preserves the momentum map $\boldsymbol{J} : P \to \mathbb{R}^3$ for any $\sigma \in \mathbb{R}$. We now proceed to determine σ such that the Hamiltonian (i.e., the total energy) is conserved along any motion $\{\boldsymbol{z}_n\}_{n=0,1,\ldots,N}$ generated by (3.7). Recall, for the system at hand the Hamiltonian $H : P \to \mathbb{R}$ is separable, of the form $H(\boldsymbol{z}) = K(\boldsymbol{p}) + V(|\boldsymbol{q}|)$ where $K(\boldsymbol{p}) = |\boldsymbol{p}|^2/2m$ is the kinetic energy of the particle. In the interval $[t_n, t_{n+1}]$ the change in kinetic energy is

$$\begin{aligned} K(\boldsymbol{p}_{n+1}) - K(\boldsymbol{p}_n) &= \frac{1}{2} m^{-1} (|\boldsymbol{p}_{n+1}|^2 - |\boldsymbol{p}_n|^2), \\ &= m^{-1} \boldsymbol{p}_{n+\frac{1}{2}} \cdot (\boldsymbol{p}_{n+1} - \boldsymbol{p}_n). \end{aligned} \tag{3.8}$$

Substituting the algorithmic equations (3.7) into the above identity yields

$$K(\boldsymbol{p}_{n+1}) - K(\boldsymbol{p}_n) = -\frac{1}{2} \sigma (|\boldsymbol{q}_{n+1}|^2 - |\boldsymbol{q}_n|^2). \tag{3.9}$$

The Hamiltonian is said to be conserved along a motion $\{\boldsymbol{z}_n\}_{n=0,1,\ldots,N}$ if $H(\boldsymbol{z}_{n+1}) = H(\boldsymbol{z}_n), \quad \forall n \geq 0$. This requires $K(\boldsymbol{p}_{n+1}) - K(\boldsymbol{p}_n) = -[V(|\boldsymbol{q}_{n+1}|) - V(|\boldsymbol{q}_n|)]$ which in view of (3.9) is satisfied by setting

$$\sigma = \frac{1}{\frac{1}{2}(|\boldsymbol{q}_{n+1}| + |\boldsymbol{q}_n|)} \frac{V(|\boldsymbol{q}_{n+1}|) - V(|\boldsymbol{q}_n|)}{|\boldsymbol{q}_{n+1}| - |\boldsymbol{q}_n|}. \tag{3.10}$$

Hence the discrete dynamics described by (3.7) together with (3.10) give rise to an algorithmic flow on P which preserves exactly the momentum map $\boldsymbol{J}$ and the Hamiltonian H.

Reduction and Stability. Due to the presence of the conserved quantity $\boldsymbol{J}$ the discrete dynamics on P defined by the energy-momentum algorithm (3.7) together with (3.10) may be reduced to the phase space $\tilde{P} \subset \mathbb{R}^2$. Carrying out an analysis identical to that for the mid-point rule yields the following results:

1) The scheme exactly preserves the relative equilibria up to group motions, i.e. preserves the fixed point in $\tilde{P}$.

2) The equilibria is unconditionally (spectrally) stable.

Approximation in the Reduced Space. The energy-momentum approximation to the reduced equations (3.4) is

$$\left.\begin{aligned} \lambda_{n+1} - \lambda_n &= \quad \Delta t m^{-1} \pi_{n+\frac{1}{2}}, \\ \pi_{n+1} - \pi_n &= -\Delta t \sigma, \end{aligned}\right\} \tag{3.11}$$

where $\sigma = [V_\mu(\lambda_{n+1}) - V_\mu(\lambda_n)]/[\lambda_{n+1} - \lambda_n]$. For this approximation we have the following results:

1) The scheme exactly preserves the fixed point in $\tilde{P}$.

2) The equilibria is unconditionally (spectrally) stable.

3.5. Numerical Verification.

In this section we present a numerical example to verify the results obtained in the preceding sections. Specifically, we consider the conservative central force problem for a particle of unit mass and radial force potential $V : \mathbb{R}_+ \to \mathbb{R}$ of the form

$$V(|\boldsymbol{q}|) = \frac{1}{2} K E^2 \quad \text{where} \quad E = \frac{1}{2}(|\boldsymbol{q}|^2 - 1). \tag{3.12}$$

For the 'stiff' case we take $K = 10^6$ and take as the amplitude of the angular momentum $\mu = 10$.

Mid-Point Approximations. To verify the result of the stability analysis of the mid-point algorithm on P we have plotted in Figure 3.1 (half) the trace of the amplification matrix $\boldsymbol{A}_{\Delta t}$ associated with the fixed point (i.e. the algorithmic relative equilibria) $\tilde{\boldsymbol{z}}^\star$ versus Ω_{F} where $\Omega_{\text{F}} = \mu \Delta t / m(\lambda^\star)^2$ is the sampling frequency associated with group motions. Since $\det[\boldsymbol{A}_{\Delta t}] \equiv 1$ the stability condition for the

algorithmic equilibria (i.e., eigenvalues on unit circle) requires $|\frac{1}{2}\,\mathrm{tr}[\boldsymbol{A}_{\Delta t}]| \leq 1$. As the plot shows, this stability condition is violated for $\Omega_{\mathrm{F}} > 2$. At the point $\Omega_{\mathrm{F}} \approx 2$ the eigenvalues of the amplification matrix experience a bifurcation from two complex-conjugate roots with unit modulus into two real roots one of which has modulus greater than unity.

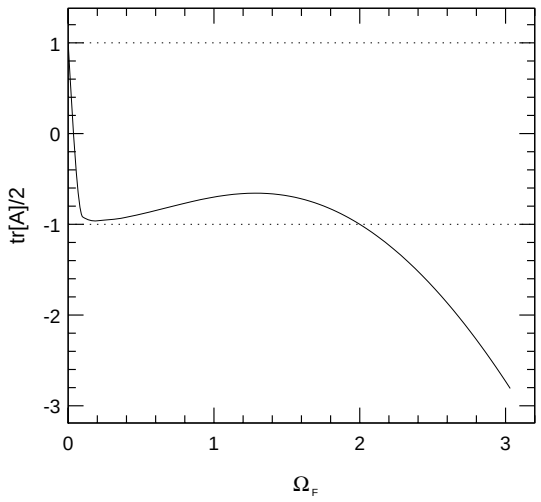

FIGURE 3.1. Trace (up to a factor of one-half) of the amplification matrix at the relative equilibria for the reduced mid-point algorithm.

For three values of Δt we integrated the equations of motion on P using (3.5) and plotted the reduced trajectories in $\tilde{P}$. Figures 3.2a-c show the fixed points in $\tilde{P}$ (i.e. the algorithmic relative equilibria) and neighboring solutions which were obtained by specifying initial conditions slightly away from the fixed points. Also shown are plots of the total energy versus time for each trajectory. For the plots of the trajectories in $\tilde{P}$ we have scaled the reduced momenta π by a factor of $1/\sqrt{mK}$ to balance the scaling between the π- and λ-axes.

Note the dependence of the location of the fixed point $\tilde{\boldsymbol{z}}^\star$ on Δt. In Figure 3.2a for $\Delta t = .01$ we have $\tilde{\boldsymbol{z}}^\star \doteq (1.0013, 0)^{\mathrm{T}}$. In Figure 3.2c for $\Delta t = .02$ the fixed point has moved to $\tilde{\boldsymbol{z}}^\star \doteq (1.0050, 0)^{\mathrm{T}}$. Also note the size of the stability region in Figure 3.2c. In this figure, curves 1-3 show the fixed point and neighboring solutions which appear qualitatively correct. Slightly further away from the fixed point we have curve 4 in which we begin to see corners in the trajectory. Finally, curve 5 shows a solution which quickly leaves the neighborhood of the fixed point and becomes a spurious solution. Figure 3.3 shows the spurious solution which results if we proceed with the computations along curve 5.

Further increases in Δt yield similar behavior, i.e., the fixed point continues to move to the right and the stability region continues to shrink. By $\Delta t = .13$ ($\Omega_{\mathrm{F}} \approx 1$) the stability region for the fixed point cannot be resolved due to the precision of the

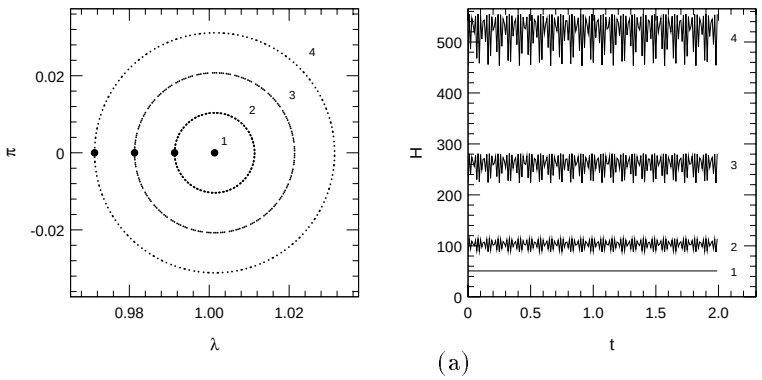

FIGURE 3.2. Reduced phase trajectories and energy plots for the mid-point algorithm on P for (a) Δt=.01 ($\Omega_{\rm F} \approx .1$), (b) $\Delta t = .015$ ($\Omega_{\rm F} \approx .15$), and (c) $\Delta t = .02$ ($\Omega_{\rm F} \approx .2$). ($\bullet$) denotes the initial condition.

computations. The fixed point itself can be maintained only for a few time steps before roundoff and tolerance errors drive the solution out of the stability region. For some value of $\Omega_{\rm F}$ between 1 and 2 the fixed point vanishes, i.e., it is lost after the first time step.

Figure 3.4 shows the result of integrating the reduced equations of motion on $\tilde{P}$ using (3.6). In this case the solution curves are independent of the time step so that we show only one plot. Here we note that the fixed point $\tilde{\boldsymbol{z}}^\star \doteq (1.0001, 0)^{\rm T}$ of the reduced dynamics is exactly preserved and that the fixed point does not have a limited stability region.

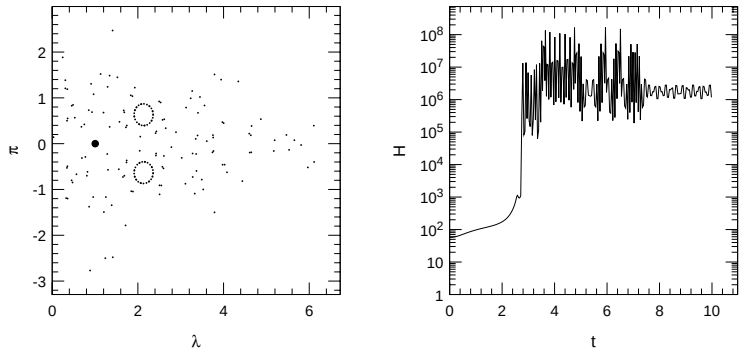

FIGURE 3.3. Spurious solution obtained by continuing computations along curve 5 of Figure 3.2. (•) denotes the initial condition.

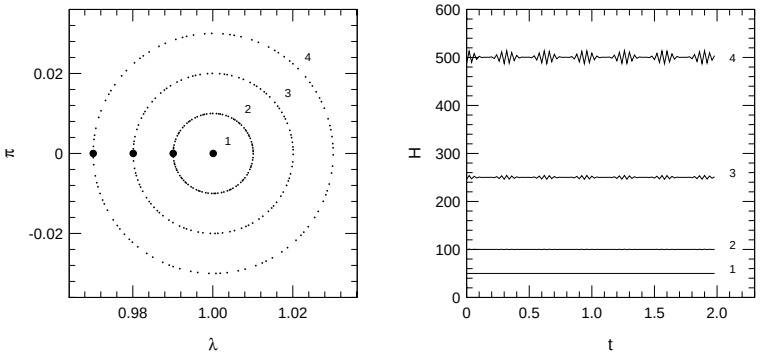

FIGURE 3.4. Phase trajectories and energy plots for the mid-point algorithm on $\tilde{P}$. Note that the trajectories are independent of Δt. (•) denotes the initial condition.

<u>*Energy-Momentum Approximations*</u>. The results of the stability analysis of the energy-momentum algorithm on P are verified in Figure 3.5 where we have plotted

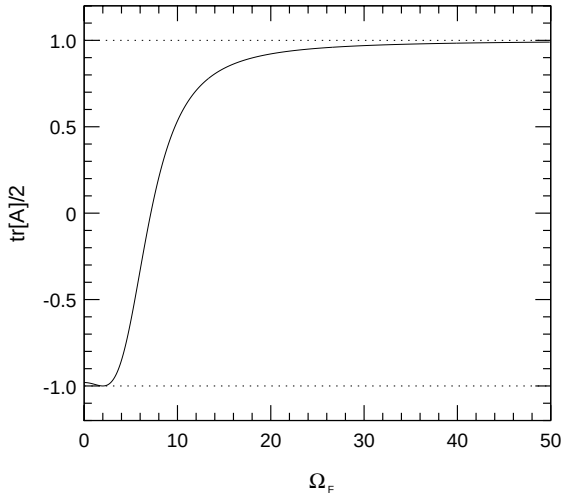

FIGURE 3.5. Trace (up to a factor of one-half) of the amplification matrix at the relative equilibria for the reduced energy-momentum algorithm.

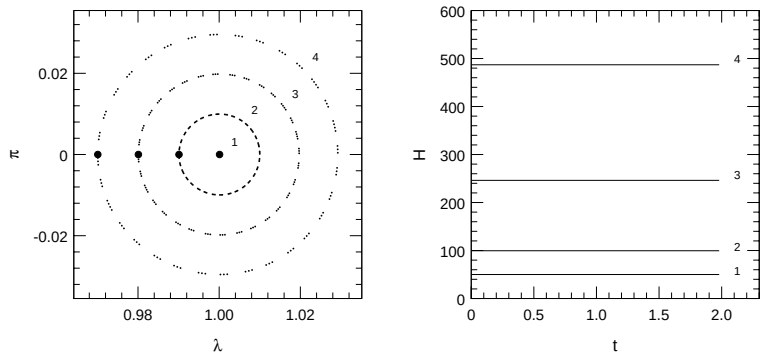

FIGURE 3.6. Reduced phase trajectories and energy plots for the energy-momentum algorithm on P. Note that the trajectories are independent of Δt. ($\bullet$) denotes the initial condition.

(half) the trace of the amplification matrix $\boldsymbol{A}_{\Delta t}$ of the fixed point (i.e. the algorithmic relative equilibria) versus Ω_{F}. For this case we also have $\det[\boldsymbol{A}_{\Delta t}] \equiv 1$ so that the stability condition becomes $|\frac{1}{2}\,\mathrm{tr}[\boldsymbol{A}_{\Delta t}]| \leq 1$. As the plot shows, the stability condition is satisfied for all $\Omega_{\mathrm{F}} \geq 0$. The only exception is $\Omega_{\mathrm{F}} = 2$ where we have $|\frac{1}{2}\,\mathrm{tr}[\tilde{\boldsymbol{A}}_{\Delta t}]| = 1$. At this point, however, we have $\boldsymbol{A}_{\Delta t} = -\mathbf{1}$ so that stability still holds.

For $\Delta t = .02$ we integrated the equations of motion on P using (3.7) together with (3.10) and plotted reduced trajectories in $\tilde{P}$. Figure 3.6 shows the fixed point and neighboring solutions as well as the energy plots for each trajectory. For the energy-momentum algorithm the location of the fixed point $\tilde{\boldsymbol{z}}^{\star} \doteq (1.0001, 0)^{\mathrm{T}}$ is exact and is independent of Δt hence we show only one plot. Also note that this algorithm is not seen to have a limited stability region which decreases with Δt as

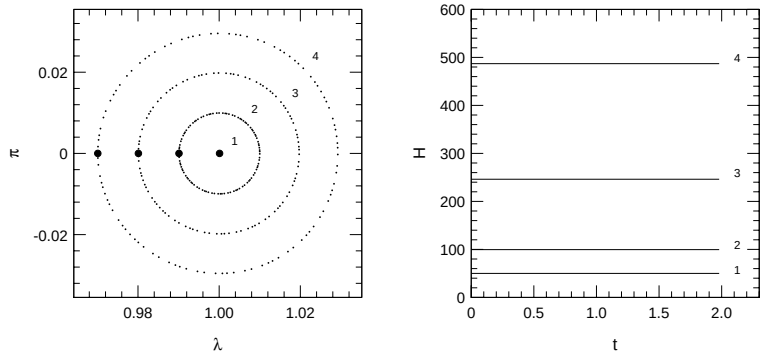

FIGURE 3.7. Phase trajectories and energy plots for the energy-momentum algorithm on $\tilde{P}$. Note that the trajectories are independent of Δt. ($\bullet$) denotes the initial condition.

does the mid-point rule on P.

Figure 3.7 shows the result of integrating the reduced equations of motion on $\tilde{P}$ using (3.11). Again, the trajectories are independent of the time step so that we show only one plot. As with the formulation on P, the fixed point $\tilde{\boldsymbol{z}}^\star \doteq (1.0001, 0)^{\mathrm{T}}$ of the reduced dynamics is exactly preserved and does not have a limited stability region. Note that the trajectories in this case are identical to those in Figure 3.6 which were obtained using the formulation on P.

4. GENERALIZATIONS.

In this section we show that the approach outlined above for the construction of exact energy-momentum conserving algorithms generalizes to more complicated systems such as nonlinear elastodynamics. (In fact, the approach generalizes to systems such as nonlinear rods and shells; see [10-11].) In particular, we outline the construction of a conserving algorithm for general frame-invariant hyperelastic models in nonlinear elasticity. For more details see [15].

As a point of departure consider the following implicit mid-point approximation to the weak form of balance of momentum

$$\begin{aligned} \frac{1}{\Delta t}\langle \boldsymbol{\pi}_{n+1} - \boldsymbol{\pi}_n, \boldsymbol{\eta}\rangle + \langle D\boldsymbol{\varphi}_{n+\frac{1}{2}}\boldsymbol{S}, \mathrm{GRAD}[\boldsymbol{\eta}]\rangle \\ = \langle \boldsymbol{f}_{n+\frac{1}{2}}, \boldsymbol{\eta}\rangle + \langle \bar{\boldsymbol{t}}_{n+\frac{1}{2}}, \boldsymbol{\eta}\rangle_\Gamma \quad \forall \boldsymbol{\eta} \in \mathcal{V}, \end{aligned} \tag{4.1a}$$

along with the local relations

$$\frac{1}{\Delta t}[\boldsymbol{\varphi}_{n+1} - \boldsymbol{\varphi}_n] = \boldsymbol{V}_{n+\frac{1}{2}} \qquad \text{and} \qquad \boldsymbol{\pi}_{n+\frac{1}{2}} = \rho_0 \boldsymbol{V}_{n+\frac{1}{2}}, \tag{4.1b}$$

where $(\cdot)_{n+\frac{1}{2}} = \frac{1}{2}[(\cdot)_n + (\cdot)_{n+1}]$ and the stress field $\boldsymbol{S}$ is left as a completely arbitrary symmetric tensor field on $\mathcal{B}$.

Recall that discrete momentum conservation follows from the *symmetry* of $\boldsymbol{S}$ independent of any constitutive relation. Hence for any symmetric field $\boldsymbol{S}$ the algorithm in (4.1a) inherits the conservation laws of linear and angular momentum from the underlying system. Given a constitutive relation for the continuum problem of the form (2.4) our goal is to construct an *algorithmic* constitutive relation, consistent with the continuum case, which leads to discrete energy conservation.

Choosing $\boldsymbol{\eta} = \boldsymbol{\varphi}_{n+1} - \boldsymbol{\varphi}_n$ in the algorithmic weak form (4.1a) and employing relations (4.1b) one arrives at the conclusion that discrete energy conservation is achieved by enforcing the local condition

$$\tfrac{1}{2}\boldsymbol{S} \cdot (\boldsymbol{C}_{n+1} - \boldsymbol{C}_n) = W(\boldsymbol{C}_{n+1}) - W(\boldsymbol{C}_n) \quad \text{in} \quad \mathcal{B}. \tag{4.2}$$

If we define the average deformation tensor $\boldsymbol{C}_{n+\frac{1}{2}}$ as

$$\boldsymbol{C}_{n+\frac{1}{2}} = \tfrac{1}{2}(\boldsymbol{C}_{n+1} + \boldsymbol{C}_n), \tag{4.3}$$

and denote by $\boldsymbol{I}$ the identity mapping on the space of symmetric second-order tensors, then a consistent approximation to a general hyperelastic constitutive relation which satisfies (4.2) is

$$\boldsymbol{S} = 2(\boldsymbol{I} - \boldsymbol{M} \otimes \boldsymbol{M}) \cdot \nabla W(\boldsymbol{C}_{n+\frac{1}{2}}) + 2\frac{W(\boldsymbol{C}_{n+1}) - W(\boldsymbol{C}_n)}{|\boldsymbol{C}_{n+1} - \boldsymbol{C}_n|}\boldsymbol{M}, \tag{4.4}$$

where $\boldsymbol{M} = \boldsymbol{C}_{n+1} - \boldsymbol{C}_n / |\boldsymbol{C}_{n+1} - \boldsymbol{C}_n|$. A simple analysis shows that (4.4) is only a Δt^2-pertubation of the mid-point approximation (2.6) and is well-defined in the limit $|\boldsymbol{C}_{n+1} - \boldsymbol{C}_n| \to 0$. In addition, for quadratic strain-energy functions such as the Saint Venant-Kirchhoff model the above expression reduces to the result given in [9]. Hence the algorithm given in (4.1a,b) together with the algorithmic constitutive equation (4.4) comprise an exact energy and momentum conserving scheme for general models in nonlinear elasticity.

5. HIGHER ORDER ACCURATE SCHEMES.

Up to now the energy-momentum algorithms we have discussed have been second-order accurate. Here we describe a time sub-stepping procedure which, for a fairly general class of second-order accurate algorithms, achieves fourth-order accuracy while retaining the stability and conservation properties of the underlying second-order method.

The proposed procedure to convert a wide class of second-order accurate time-stepping methods into fourth-order accurate methods is remarkably simple. Given a second-order accurate scheme, the procedure requires the execution of three fractional

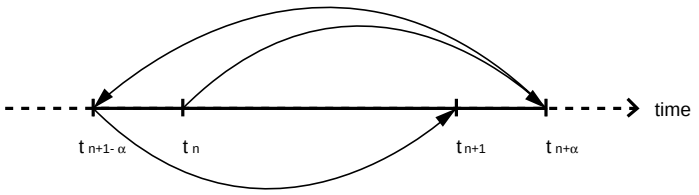

FIGURE 5.1. To advance by one fourth-order accurate time step requires the successive execution of three fractional steps with the second-order method.

steps of sizes $\alpha\Delta t, (1-2\alpha)\Delta t$ and $\alpha\Delta t$, respectively, in order to advance one time step of size Δt. An illustration of the technique is given in Figure 5.1.
The constant α is independent of the time-stepping method to which the procedure is applied. Its numerical value and the precise statement of this result are summarized in the following.

Let $\boldsymbol{f}$ be a smooth function on $\mathbb{R}^n \times [0,T]$, where $[0,T]$ is a time interval of interest and consider the general initial value problem

$$\left.\begin{aligned} \dot{\boldsymbol{y}}(t) &= \boldsymbol{f}(\boldsymbol{y}(t),t), \\ \boldsymbol{y}|_{t=0} &= \boldsymbol{y}_0\,. \end{aligned}\right\} \tag{5.1}$$

Suppose a given algorithm to solve the initial value problem (5.1) is of the form

$$\begin{aligned} \boldsymbol{y}_{n+1} - \boldsymbol{y}_n = \Delta t\, \tilde{\boldsymbol{f}}(\boldsymbol{y}_n, \boldsymbol{y}_{n+1}, t_n, t_{n+1}) \\ + \boldsymbol{\beta}\Delta t^2 [\boldsymbol{f}_{,t}(\boldsymbol{y}_{n+1}, t_{n+1}) - \boldsymbol{f}_{,t}(\boldsymbol{y}_n, t_n)], \end{aligned} \tag{5.2}$$

where the subscripts $(\cdot)_n$ and $(\cdot)_{n+1}$ refer to algorithmic approximations of $\boldsymbol{y}(t_n)$ and $\boldsymbol{y}(t_{n+1})$, respectively, $\boldsymbol{\beta}$ is a diagonal matrix of free algorithmic parameters (for many methods $\boldsymbol{\beta} \equiv \boldsymbol{0}$) and $\tilde{\boldsymbol{f}}(\boldsymbol{y}_n, \boldsymbol{y}_{n+1}, t_n, t_{n+1})$ satisfies the following conditions:

$$\left.\begin{aligned} \tilde{\boldsymbol{f}}(\boldsymbol{y},\boldsymbol{y},t,t) &= \boldsymbol{f}(\boldsymbol{y},t), \quad \forall \boldsymbol{y}, t; \\ \tilde{\boldsymbol{f}}(\boldsymbol{y},\boldsymbol{x},s,t) &= \tilde{\boldsymbol{f}}(\boldsymbol{x},\boldsymbol{y},t,s). \end{aligned}\right\}$$

Then the method can be transformed into a fourth-order accurate method by using the mentioned sub-stepping procedure with

$$\alpha = \frac{1}{3}\left(2 + 2^{-\frac{1}{3}} + 2^{\frac{1}{3}}\right).$$

Successive applications of a second-order method with different time-step sizes to attain fourth-order accuracy in a macro step yields a convenient scheme with a number of attractive features over conventional fourth-order accurate algorithms. For more details see [16].

6. CLOSING REMARKS.

We have provided a review of recent results on symplectic and conserving time-stepping algorithms for Hamiltonian systems, in particular, stiff systems with symmetry. Based on numerical evidence within the context of relatively complex systems and analytical evidence within the context of a simple model problem we conclude that seemingly ideal symplectic schemes such as the Gauss family of algebraically stable implicit Runge-Kutta methods are not suitable for the systems of interest. In particular, these algorithms lose their effectiveness as implicit schemes since they exhibit spurious solutions and/or blow-up when high frequencies are ignored in the presence of large group motions. Within the context of a simple model problem recent results show that the cause of the instability is an artificial coupling between group motions and internal motions. Results show that instability may be precluded by symplectic reduction or by alternative conserving schemes, the latter being the most practical solution in general.

7. REFERENCES.

[1] R. de Vogelaere (1956) "Methods of Integration which Preserve the Contact Transformation Property of Hamiltonian Equations," *Department of Mathematics, University of Notre Dame,* Report **4**.

[2] Feng Kang (1986) "Difference Schemes for Hamiltonian Formalism and Symplectic Geometry," *J. Computational Mathematics,* **4**, 279–289.

[3] J.M. Sanz-Serna (1988) "Runge-Kutta Schemes for Hamiltonian Systems," BIT, **28**, 877–883.

[4] J.M. Sanz-Serna (1992) "The Numerical Integration of Hamiltonian Systems," Proceedings of the Conference on Computational Differential Equations, Imperial College, London, 3–7 July 1989, in press.

[5] H. Yoshida (1993) "Recent Progress in the Theory and Application of Symplectic Integrators," *Celestial Mechanics and Dynamical Astronomy,* **56**, 27–43.

[6] A. Bayliss & E. Isaacson (1975) "How to Make Your Algorithm Conservative," *American Mathematical Society*, A594–A595.

[7] R.A. Labudde & D. Greenspan (1976a) "Energy and Momentum Conserving Methods of Arbitrary Order for the Numerical Integration of Equations of Motion. Part I," *Numerisch Mathematik*, **25** (1976a) 323–346.

[8] R.A. Labudde & D. Greenspan (1976b) "Energy and Momentum Conserving Methods of Arbitrary Order for the Numerical Integration of Equations of Motion. Part II," *Numerisch Mathematik*, **26**, 1–16.

[9] J.C. Simo & N. Tarnow (1992a) "The Discrete Energy-Momentum Method. Conserving Algorithms for Nonlinear Elastodynamics," *ZAMP,* **43**, 757–793.

[10] J.C. Simo & N. Tarnow (1992b) "A New Energy-Momentum Method for the Dynamics of Nonlinear Shells," *International J. Numerical Methods in Engineering,* in press.

[11] J.C. Simo, N. Tarnow & M. Doblaré (1993) "Exact Energy-Momentum Algorithms for the Dynamics of Nonlinear Rods," *International J. Numerical Methods in Engineering,* in press.

[12] J.C. Simo & O. Gonzalez (1993) "Assessment of Energy-Momentum and Symplectic Schemes for Stiff Dynamical Systems," *American Society of Mechanical Engineers,* ASME Winter Annual Meeting, New Orleans, Louisiana.

[13] Ge Zhong & J.E. Marsden (1988) "Lie-Poisson Hamilton-Jacobi Theory and Lie-Poisson Integrators," *Physics Letters A,* **3**, 134–139.

[14] O. Gonzalez & J.C. Simo (1994) "On the Stability of Symplectic and Energy-Momentum Algorithms for Nonlinear Hamiltonian Systems with Symmetry," *Computer Methods in Applied Mechanics and Engineering,* submitted.

[15] O. Gonzalez & J.C. Simo (1994) "Exact Energy-Momentum Conserving Algorithms for General Models in Nonlinear Elasticity," *Computer Methods in Applied Mechanics and Engineering,* in preparation.

[16] N. Tarnow & J.C. Simo (1993) "How to Render Second-Order Accurate Time-Stepping Algorithms Fourth-Order Accurate While Retaining the Stability and Conservation Properties," *Department of Mechanical Engineering, Division of Applied Mechanics, Stanford University*, Technical Report.